# Full ninedimensional ab initio potential energy surfaces and trajectory studies of A band photodissociation dynamics: CH3I*→CH3+I, CH3+I*, and CD3I*→CD3+I, CD3+I*

Yoshiaki Amatatsu, Satoshi Yabushita, and Keiji Morokuma

Citation: The Journal of Chemical Physics **104**, 9783 (1996); doi: 10.1063/1.471758
View online: http://dx.doi.org/10.1063/1.471758
View Table of Contents: http://scitation.aip.org/content/aip/journal/jcp/104/24?ver=pdfcov
Published by the AIP Publishing

# Full nine-dimensional *ab initio* potential energy surfaces and trajectory studies of *A*-band photodissociation dynamics: $CH_3I^* \rightarrow CH_3+I$, $CH_3+I^*$, and $CD_3I^* \rightarrow CD_3+I$, $CD_3+I^*$

Yoshiaki Amatatsu
*Department of Chemistry, Akita University, Tegata Gakuen-cho, Akita 010, Japan, and Institute for Molecular Science, Myodaiji, Okazaki 444, Japan*

Satoshi Yabushita
*Department of Chemistry, Faculty of Science and Technology, Keio University, Hiyoshi, Kohoku-ku, Yokohama 223, Japan, and Institute for Molecular Science, Myodaiji, Okazaki 444, Japan*

Keiji Morokuma
*Cherry L. Emerson Center for Scientific Computation and Department of Chemistry, Emory University, Atlanta, Georgia 30322, and Institute for Molecular Science, Myodaiji, Okazaki 444, Japan*

(Received 19 December 1995; accepted 12 March 1996)

The full nine-dimensional potential energy surfaces (PESs) of the $^3Q_0$ and $^1Q_1$ states of $CH_3I$ have been calculated with the *ab initio* contracted spin–orbit configuration interaction method. The results are fitted to three diabatic potential terms and their couplings as functions of all the internal degrees of freedom. The transition dipole at the Franck–Condon region has also been calculated. Surface hopping quasiclassical trajectory calculations on these potential energy surfaces have been performed to examine the photodissociation dynamics of both $CH_3I$ and $CD_3I$ in the *A*-continuum. The results are in general good agreement with the recent experimental findings. The reasonable $I^*/(I^*+I)$ branching ratio can be obtained with these PESs when the contribution of direct transition to the $^1Q_1$ state is considered. The rotational distribution of the $CH_3$ and $CD_3$ fragments and its $I^*/(I^*+I)$-channel selectivity are determined by the shape of the PESs with respect to the bending angle outside the conical intersection region. The vibrational distribution of umbrella mode is closely related to the shape of PESs for the umbrella angle; the sudden switch of reaction coordinate from $^3Q_0$ to $^1Q_1$ at the conical intersection is the origin of vibrational excitation in the $I^*$ channel. The larger umbrella excitation of the $CD_3$ fragment in both I and $I^*$ channels, in comparison with the $CH_3$ fragment, is related to the larger separation of the reaction coordinate from the Franck–Condon geometry. The symmetric stretching energy increases during the dissociation, which is related to the shape of PESs with respect to this coordinate, and the excitation of symmetric stretching mode seems to be possible. © *1996 American Institute of Physics.*
[S0021-9606(96)00523-5]

## I. INTRODUCTION

The photodissociation reaction in the *A*-continuum ($n \rightarrow \sigma^*$) of $CH_3I$, with two reaction channels $CH_3I^* \rightarrow CH_3+I(^2P_{3/2})$ (I-channel) and $CH_3+I^*(^2P_{1/2})$ ($I^*$-channel), has recently been a subject of great interest from both experimental[1–34] and theoretical[35–53] points of view. Up to 10 years ago, this photodissociation had been characterized as the reaction that the umbrella mode of the $CH_3$ fragment exhibits an inverted population and $I^*$ is preferentially produced.[8–13,35–36] The widely accepted interpretation had been that a large geometrical change of the $CH_3$ part between the equilibrium and the dissociation limit of $CH_3I$ caused vibrational excitation of the umbrella motion. However, during the last 10 years, many experimental findings which contradict this traditional interpretation have been reported[14–32] and a new picture of the reaction mechanism has been required. We have performed *ab initio* spin–orbit configuration interaction (SOCI) calculations[47] and constructed six-dimensional potential energy surfaces (PESs) in lower excited states.[48] From the characteristics of these PESs and semiclassical surface-hopping trajectories, we have provided a new interpretation for these recent experimental findings, such as the hot rotational distribution of the $CH_3$ product in the I channel and the cold distribution in the $I^*$ channel, and the hot distribution in the umbrella vibration for the $CH_3$ product in the I channel and the cold distribution in the $I^*$ channel. Recently a wave packet simulation has been performed on our *ab initio* PESs.[51]

However, in our previous paper,[48] we did not discuss the following problems which still remain to be solved.

(i) Mass effect on the photodissociation dynamics, i.e., the difference between $CH_3I$ and $CD_3I$ reactions.
(ii) The possibility of excitation of the symmetric stretching ($v_1$) mode of the $CH_3$ fragment.
(iii) The character of transitions from the ground to the excited states, $^3Q_{0+}$, $^1Q_1$, and $^3Q_1$.

At first, we would like to make a brief review on these problems. Mass effect of the photodissociation provides a unique opportunity to probe details of dynamics of the pro-

cess and various experimental techniques have been applied to $CD_3I$ as well as $CH_3I$ photodissociation to examine I*/(I*+I) ratio, the vibrational excitation of the umbrella mode, the rotational excitation of the $CH_3$ fragment.[10–15,18,19,22–24,26] The I*/(I*+I) branching ratio of $CD_3I$ photodissociation ($\sim$0.8) is in general larger than that of $CH_3I$($\sim$0.7), except in the low energy region below 300 nm. The finding is contrary to the intuitive prediction that, because of the heavier mass, the photodissociation of $CD_3I$ takes place more adiabatically than that of $CH_3I$ and therefore $CD_3I$ should more easily produce I in the ground state. Guo made a comment on this discrepancy and pointed out the relative importance of the bending motion.[42]

The vibrational excitation of the umbrella mode of $CH_3$ (or $CD_3$) has attracted a greatest attention since the early days of research of this reaction.[13] In earlier studies, the inverted population in the umbrella mode was found for both I and I*-channel product. More recent experiments have shown, however, that, although the I-channel product has an inverted population, the population of the I*-channel product is not inverted. We have shown in our previous study[48] that, after the electronic excitation from the ground state to $^3Q_0$, the umbrella motion of the I*-channel product is adiabatically relaxed through the dissociation process to reach the dissociation limit. On the other hand, the umbrella motion of the I-channel product is suddenly excited upon passing through the conical intersection from the $^3Q_0$ to the $^1Q_1$ state because of a sudden change of the reaction coordinate. The mass effect on the umbrella motion excitation has been experimentally studied. The vibrational population of $CD_3$, for instance, 4:3:2 for $v_2=0:1:2$ by Hall *et al.*[29] and 1.1:1 for $v_2=0:2$ by Houston *et al.*,[24] is hotter than that of $CH_3$, for instance, 66:26:8 for $v_2=0:1:2$ by Suzuki *et al.*[27] and 1:0.27 for $v_2=0:1$ by Zahedi *et al.*[30] The third point of the mass effect is related to the rotational excitation of $CH_3$ (or $CD_3$) product. As reported many times experi mentally[18,19,21,22,24,34] and theoretically,[48,51] the I-channel product is rotationally excited around the axis perpendicular of the top axis of $CH_3$ (or $CD_3$), while the I*-channel product is rotationally much colder. The rotational temperature of $CH_3$ ($v_2=0$) and $CD_3$ ($v_2=0$) in the I-channel is estimated to be $120\pm30$ and $105\pm30$ K, respectively, by Houston *et al.*,[24] and the average rotational energy to be 104 $cm^{-1}$ for $CH_3$ and 94 $cm^{-1}$ for $CD_3$ by Chandler *et al.*[22]

The possibility of the excitation of the symmetric stretching ($\nu_1$) mode of $CH_3$ (or $CD_3$) product is considered unlikely in earlier days, because the vibrational frequency is too high ($\sim$3000 $cm^{-1}$) to excite. However, such a possibility has been pointed out by some groups. Powis and Black have reported that the symmetric stretching excitation has both isotope and channel specificity, i.e., only $CD_3$ in the I-channel is excited.[19] They tentatively gave an interpretation that the vibrational level at $v_1=1$ was near resonance with the vibrational level with four quanta in the umbrella mode. Houston *et al.* have reported that $CH_3$ is excited but there is no channel selectivity.[24] Chandler *et al.* have found that the I-channel product is preferentially excited to $v_1=1$ over the I*-channel and the I*/(I*+I) ratio was estimated to be $>2.0$ for $CH_3I$ (Ref. 20) and $1.3\pm0.2$ for $CD_3I$.[21]

The character of transition from the ground to the excited states is an important clue to some mysteries of the photodissociation dynamics of $CH_3I$. Transitions to the $^3Q_1$, $^3Q_0$, and $^1Q_1$ states are allowed in the *A*-continuum of $CH_3I$. Gedanken and Rowe have carried out the magnetic circular dichroism (MCD) experiment at the *A*-continuum to find the relative intensity of $^3Q_0:{}^1Q_1:{}^3Q_1 = 75:25:1$; especially, in the 260–262 nm region, the transition is almost exclusively parallel (94%), i.e., to the $^3Q_{0+}$ state.[5] Hunter and Kristjanssen have concluded based on a photoacoustic measurement that the transition of $CH_3I$ is mainly $^3Q_{0+}$ at 248 nm, and the parallel component is due to the strong coupling with the $^3Q_0$ state.[7] Pipes *et al.* also have concluded that the parallel transition is dominant at 266 nm, based on the determination of transition dipole matrix elements for 266 nm photofragmentation of $|JKM\rangle$ state-selected $CD_3I$.[33] The anisotropy parameter is also important to discuss the character of transition. Several have reported that the transition is mainly to the $^3Q_0$ state and the production of I($^2P_{3/2}$) is exclusively caused by the curve crossing.[12,13,17,23] Very recently, however, photolysis in the low energy region in the *A*-continuum, i.e., below 300 nm, were carried out to examine the character of the transition. Fairbrother *et al.* pointed out the importance of the perpendicular transition to $^3Q_1$, where exclusively produces $CH_3+I$.[31] Hertz and Syage have reported that the transition has a small perpendicular character, $\sigma_\perp/\sigma_\parallel=0–0.1$ for 266 nm and 0.2–0.3 for 304 nm; in the high and medium energy region of the *A*-continuum where most of photolysis experiments have been performed, the perpendicular component contributes little, while in the lower energy region, it becomes more important.[32]

In the present study, we mainly discuss the photodissociation dynamics to which we did not refer in our previous study, based on the surface hopping quasiclassical trajectory calculation using the nine dimensional PESs. In Sec. II, we discuss the method of calculation for obtaining the adiabatic potential energy and transition dipole function, the transformation from the adiabatic to the diabatic basis, and analytical fitting of diabatic energies and the method of surface hopping quasiclassical trajectory calculation. In Sec. III, we discuss at first the character of transitions from the ground to excited states and then the global features of the PES of $^1Q_1$ and $^3Q_0$, with the emphasis on the CH stretching mode and on the difference between $CH_3I$ and $CD_3I$ umbrella motion. We also discuss the mass effect on the I*/(I*+I) branching ratio, the rotational excitation, the umbrella mode excitation, and the possible symmetric stretching excitation in $CD_3$ as well as in $CD_3$. Finally, in Sec. IV, we give our conclusions.

## II. METHODS OF CALCULATION

### A. Adiabatic energies

*Ab initio* spin–orbit configuration interaction (SOCI) calculations have been performed for the ground and lower

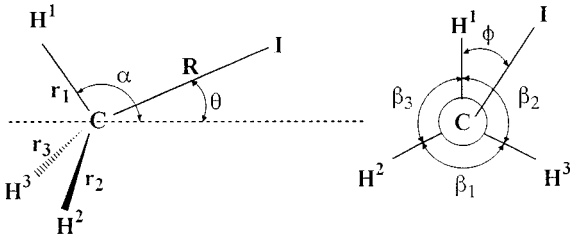


FIG. 1. The definition of internal coordinates. The broken line on the left is the axis for which the umbrella angle is equal for all three CH's. This axis is defined as the $z$-axis in body-fixed coordinate. The figure on the right is projection to the plane perpendicular to this axis. $\theta$ takes a value between 0 and $\pi$, and $\phi$ is between 0 and $2\pi$. $\beta_i$'s are redundant, satisfying $\beta_1+\beta_2+\beta_3=2\pi$.

excited states of $CH_3I$ to obtain the nine dimensional PESs including all the internal degrees of freedom, using a modified COLUMBUS package[52(a)] implemented with our own SOCI code.[52(b)] To save the computational time, we adopted the ''contracted'' SOCI method which considered the spin–orbit interaction only among the lowest $^1A_1$, $^3E$, $^1E$, and $^3A_1$ spin–orbit free states after large scale spin–orbit free CI calculations. The method, details of which were described in our previous paper, was found to reproduce the results of full SOCI results very accurately.[47] The basis sets and the details of calculation are the same with those in our previous paper[48] and will not be repeated. In addition to those geometrical points we previously obtained for six dimensional PESs,[48] in the present study we have newly calculated 182 points to describe the CH stretching modes and their couplings with the other modes, using the internal coordinates defined in Fig. 1. The calculated equilibrium geometry in the ground state of $CH_3I$ with $C_{3v}$ symmetry has the CI distance of $R_e=4.040\,95$ a.u., the CH distance of $r_e=2.065\,73$ a.u. and $\alpha=108.5$ deg. At a large separation $CH_3$–I distance of $R=100$ a.u., we also calculated the $CH_3$ equilibrium geometry with $D_{3h}$ symmetry to have the CH distance of $r_e^{\infty}=2.052\,66$ a.u. All the distances and energies in the present papers are in atomic units unless otherwise mentioned.

### B. Transformation from the adiabatic to the diabatic basis

To run a classical trajectory calculation, we have to evaluate the $^3Q_0$ and $^1Q_1$ PESs. However, it is hard to fit them directly to analytical functions with respect to the internal coordinates of $CH_3I$ because the character of adiabatic states changes with geometry. We transformed the adiabatic to the diabatic energies to make them easier to fit to analytical functions. The details of the method are already published.[48] With this method, three adiabatic states, $\Psi_1(^1Q_1)$, $\Psi_2(^1Q_1)$, and $\Psi_3(^3Q_0)$, were transformed into three adiabatic states, which are approximately $^1\Phi_1 \approx \Psi_1[^1Q_1(A')]$, $^1\Phi_{12} \approx \Psi_2[^1Q_1(A'')]$, and $^3\Phi_{13} \approx \Psi_3(^3Q_{0+})$ in $C_s$ double group.[53] The essential point of this transformation is to minimize the minor spin component for each diabatic state. This way we obtained six diabatic potential terms, $V_1$, $V_2$, $V_3$, $V_{12}$, $V_{13}$, and $V_{23}$, where $V_1$, $V_2$, and $V_3$ are the energies of the diabatic states, $^1\Phi_1$, $^1\Phi_2$, and $^3\Phi_3$, respectively, and $V_{12}$, $V_{13}$, and $V_{23}$ are the couplings between these states.

### C. Analytical fitting of diabatic potential terms

We have fitted the six diabatic matrix elements to analytical functions with respect to ten internal coordinates (including one redundancy), defined in Fig. 1. As mentioned in our previous paper, three diagonal terms in practice obey an energetic and symmetry hierarchy rule with respect to the internal coordinates,[48] and this is true even if three CH stretching coordinates are included. The diagonal terms change within 0.1 a.u. with respect to $R$, within 0.01 a.u. with respect to $r_i$'s as well as $\alpha$, and within 0.001 a.u. with respect to the other parameters in the region probed by classical trajectories. This difference in the magnitude of energy leads to an additivity rule among the internal coordinates, i.e., the diagonal terms can in practice be expressed as a sum of five terms which include only the relevant internal coordinates; (i) the $R$ and $\alpha$ term, which is the largest contribution to the diabatic energy, (ii) the $CH_3$ stretching term which relates to the $r_i$'s and their couplings with $R$ and $\alpha$, (iii) the term including the bending angle $\theta$ and its direction $\phi$ of the I atom and their couplings with $R$ and $\alpha$, (iv) the $CH_3$ deformation term which contains the $\beta_i$'s and their couplings with $R$ and $\alpha$, and (v) the $CH_3$ force field in the dissociation limit. Furthermore, in case of the diabatic triplet correlating to $CH_3+I^*$ ($V_3$ in our definition), there is the constant term which is the energy difference between the ground ($^2P_{3/2}$) and the excited ($^2P_{1/2}$) states of the iodine atom, $\Delta E_1=0.034\,646$ a.u. These five terms can be separately fitted to analytical functions with respect to only the relevant internal coordinates.

Before doing actual fitting, we have to consider the requirement that the adiabatic energies $^3Q_0$ and $^1Q_1$ are unchanged by permutation among the three hydrogens, which is related to the internal coordinates $\phi$, $\beta_i$'s and $r_i$'s. This means that every term, (i)–(v) above, in each diabatic matrix element, $V_1$, $V_2$, $V_3$, $V_{13}$, $V_{23}$, and $V_{12}$, have to satisfy this permutation requirement. We have analyzed the requirement in detail for seven internal coordinates in the previous paper.[48] Additional consideration is needed when three CH distances are included and the required form is discussed in the Appendix.

First, we made the fifth term, the force field of $CH_3$ in the dissociation limit with $D_{3h}$ symmetry. The potential functions of $CH_3$ we used is

$$V_{CH_3}=k_{22}x^2+k_{24}x^4+(1/2)k_1S_1^2+(1/2)k_4(S_{4a}^2+S_{4b}^2)+(1/2)k_5(S_{5a}^2+S_{5b}^2), \quad (1)$$

where $x=r_e^{\infty}\sin\Delta\alpha$, $\Delta\alpha=\alpha-\pi/2$, $S_1=(1/\sqrt{3})(\Delta r_1+\Delta r_2+\Delta r_3)$,

$$S_{4a}=(1/\sqrt{6})(2\Delta r_1-\Delta r_2-\Delta r_3),$$

$$S_{4b}=(1/\sqrt{2})(\Delta r_2-\Delta r_3),$$

$$\Delta r_i = r_i - r_e^{\infty} \quad (i=1,2,3),$$

$$S_{5a} = (1/\sqrt{6})(2\Delta\beta_1 - \Delta\beta_2 - \Delta\beta_3),$$

$$S_{5b} = (1/\sqrt{2})(\Delta\beta_2 - \Delta\beta_3),$$

$$\Delta\beta_i = \beta_i - 2\pi/3 \quad (i=1,2,3).$$

The coupling terms, $S_{4a}S_{5a}$ and $S_{4b}S_{5b}$, are small and are neglected in $V_{CH_3}$. One can see easily that $V_{CH_3}$ satisfies with the permutation requirement.

Next we fitted the other four terms, (i)–(iv) above, of each diagonal matrix element. We have used more flexible functional forms from the previous ones,[48] so that a good fit can be obtained not only in the classically probed region but also in the region which is away from it. The actual functional forms are adopted as follows:

$$V_1 = (A_0 + A_1\Delta R + A_2\Delta R^2 + A_3^*)\exp(-A_4\Delta R) + (A_5 + A_6^* \cos\theta)S_1 \exp(-A_4\Delta R) + [A_7^*(\cos\theta - 1) + A_8(\cos 2\theta - 1) + (A_3^* - A_7^*)(\cos 3\theta - 1) + A_9 X \sin\theta]\exp(-A_4\Delta R) + (A_{10} + A_{11}^* \cos\theta)S_{5a}\exp(-A_4\Delta R) + V_{CH_3}, \quad (2)$$

$$V_2 = (A_0 + A_1\Delta R + A_2\Delta R^2 + A_3^*)\exp(-A_4\Delta R) + (A_5 + A_6^* \cos\theta)S_1 \exp(-A_4\Delta R) + [A_7^*(\cos\theta - 1) + A_8(\cos 2\theta - 1) + (A_3^* - A_7^*)(\cos 3\theta - 1) - A_9 X \sin\theta]\exp(-A_4\Delta R) - (A_{10} + A_{11}^* \cos\theta)S_{5a}\exp(-A_4\Delta R) + V_{CH_3}, \quad (3)$$

$$V_3 = (B_0 + B_1\Delta R + B_2\Delta R^2 + B_3^*)\exp(-B_4\Delta R) + (B_5 + B_6^* \cos\theta)S_1 \exp(-B_4\Delta R) + [B_7^*(\cos\theta - 1) + B_8(\cos 2\theta - 1) + (B_3^* - B_7^*)(\cos 3\theta - 1) + B_9 X \sin\theta]\exp(-B_4\Delta R) + (B_{10} + B_{11}^* \cos\theta)S_{5a}\exp(-B_4\Delta R) + V_{CH_3} + \Delta E_I, \quad (4)$$

where

$$\Delta R = R - R_e,$$

$$X(\phi,\beta_2,\beta_3,\zeta) = \{\cos(3\phi+\zeta) + \cos[3(\phi+\beta_3)+\zeta] + \cos[3(\phi-\beta_2)+\zeta]\}/3,$$

$$\tan\zeta = \tan(\zeta_1+\zeta_2), \quad \tan\zeta_1 = S_{5b}/S_{5a},$$

$$\tan\zeta_2 = S_{4b}/S_{4a}.$$

The coefficients $A_i$'s and $B_i$'s without $*$, represented in general by $P_i$, are the following functions of $\Delta\alpha$:

$$P_i = P_{i0} + P_{i1}\cos\Delta\alpha + P_{i2}\cos 2\Delta\alpha. \quad (5)$$

The coefficients $A_i$'s and $B_i$'s with $*$, represented in general by $Q_i$, are the following functions of $\Delta\alpha$:

$$Q_i = Q_{i0} + Q_{i1}\sin\Delta\alpha + Q_{i2}\sin 2\Delta\alpha. \quad (6)$$

The first and second lines on the right-hand side of Eqs. (2) and (3), which relate to only $R$, $\alpha$, and $S_1$, are the same because $V_1$ and $V_2$ are degenerate in $C_{3v}$ symmetry. The second lines in Eqs. (2)–(4), relating to the symmetric CH stretch, are all assumed to have the same functional form which is the first order with respect to $S_1$. The third lines, relating to the direction of bending of the I atom, are different from each other, though they share the common exponential factor $A_4$ for a convenience in fitting. The fourth lines in Eqs. (2)–(4), relating to the $CH_3$ deformation, are functions of $S_{5a}$ and differ only in sign between Eqs. (2) and (3). Although the fourth line of $V_3$ also contains a formal dependence on $S_{5a}$, the actual dependency was found to be small and, therefore, $B_{10}$ and $B_{11}$ are set to zero. We found that the diabatic diagonal elements do not change with $S_{4a}$ and thus no functional dependency is included in Eqs. (2)–(4) except for the $V_{CH_3}$ part. The fifth lines in Eqs. (2) and (4) describe the force field of $CH_3$ in the dissociation limit. Furthermore, the constant $\Delta E_I$ is added to the fifth line in Eq. (4). The fitted coefficient sets of the diagonal terms are listed in Table I.

Next we discuss the fitting forms of the off-diagonal elements, which also obey the additivity rule. The actual functional forms used are shown in Eqs. (7)–(9),

$$V_{13} = (D_1 \sin\theta + D_2^* \sin 2\theta)X/[(R-D_3)^2 + D_4^2] + (D_5 + D_6^* \cos\theta)S_{5a}/[(R-D_3)^2 + D_4^2] + (D_7 + D_8^* \cos\theta)S_{4a}/[(R-D_3)^2 + D_4^2], \quad (7)$$

$$V_{23} = -(D_1 \sin\theta + D_2^* \sin 2\theta)Y/[(R-D_3)^2 + D_4^2] - (D_5 + D_6^* \cos\theta)S_{5b}/[(R-D_3)^2 + D_4^2] - (D_7 + D_8^* \cos\theta)S_{4b}/[(R-D_3)^2 + D_4^2], \quad (8)$$

$$V_{12} = A_9 \sin\theta Y \exp(-A_4\Delta R) + (A_{10} + A_{11}^* \cos\theta)S_{5b}\exp(-A_4\Delta R), \quad (9)$$

where

$$Y(\phi,\beta_2,\beta_3,\zeta) = \{\sin(3\phi+\zeta) + \sin[3(\phi+\beta_3)+\zeta] + \sin[3(\phi-\beta_2)+\zeta]\}/3.$$

These off-diagonal elements are all zero within the $C_{3v}$ symmetry. Since the diabatic states $^1\Phi_1$ and $^1\Phi_2$ belong to $A'$ and $A''$ in $C_s$ symmetry, respectively, $V_{23}$ is 0 in the $C_s$ symmetry, whereas $V_{13}$ is nonzero even in $C_s$. The singlet–triplet coupling terms $V_{13}$ and $V_{23}$ have been found to be reproduced well by Lorentzian functions which have the maximum with respect to $R$ near the conical intersection.

TABLE I. Potential function parameters; coefficients of diagonal terms (in a.u.).

| | $P_{i0}$ | $P_{i1}$ | $P_{i2}$ |
|---|---|---|---|
| $A_0$ | 0.231 308 | −0.066 421 | −0.031 709 |
| $A_1$ | −0.109 315 | 0.142 368 | 0.004 171 |
| $A_2$ | 0.019 901 | −0.022 302 | 0.0 |
| $A_4$ | 1.718 200 | −0.162 716 | 0.128 111 |
| $A_5$ | −0.032 418 | 0.031 726 | 0.0 |
| $A_8$ | −0.072 448 | 0.077 366 | −0.047 205 |
| $A_9$ | −0.004 848 | −0.001 324 | 0.000 381 |
| $A_{10}$ | −0.009 842 | 0.007 512 | 0.0 |
| $B_0$ | 0.150 334 | −0.031 513 | −0.022 155 |
| $B_1$ | −0.119 258 | 0.064 387 | 0.016 015 |
| $B_2$ | 0.113 208 | −0.139 262 | 0.0 |
| $B_4$ | 0.938 154 | 0.276 679 | 0.028 479 |
| $B_5$ | −0.057 911 | 0.057 376 | 0.0 |
| $B_8$ | −0.051 651 | −0.131 315 | 0.089 466 |
| $B_9$ | 0.0 | 0.0 | 0.0 |
| $B_{10}$ | 0.0 | 0.0 | 0.0 |
| | $Q_{i0}$ | $Q_{i1}$ | $Q_{i2}$ |
| $A_3^*$ | 0.0 | −0.322 354 | 0.096 945 |
| $A_6^*$ | 0.0 | 0.224 101 | −0.141 370 |
| $A_7^*$ | 0.0 | −0.283 743 | 0.055 896 |
| $A_{11}^*$ | 0.0 | 0.006 063 | −0.002 086 |
| $B_3^*$ | 0.0 | −0.316 726 | 0.086 647 |
| $B_6^*$ | 0.0 | 0.220 449 | −0.142 314 |
| $B_7^*$ | 0.0 | −0.290 132 | −0.001 569 |
| $B_{11}^*$ | 0.0 | 0.0 | 0.0 |

| | | | | | |
|---|---|---|---|---|---|
| $k_{22}$ | 0.012 559 | $k_{24}$ | 0.026 533 | | |
| $k_1$ | 0.388 582 | $k_4$ | 0.395 720 | $k_5$ | 0.102 706 |

The off-diagonal term $V_{12}$ between the two singlet states has been found to fit well to the function relating to the $\phi$ and $\beta_i$ parts of the diagonal element $V_1$ (or $V_2$) and satisfies the permutation requirement as pointed out before. The coefficients $D_i$ without $*$ are also given in the form of Eq. (5) and the coefficients $D_i^*$ with $*$ in the form of Eq. (6), both as functions of $\Delta\alpha$. The fitted coefficient sets of the off-diagonal elements are listed in Table II.

TABLE II. Potential function parameters; coefficients of off-diagonal terms (in a.u.).

| | $P_{i0}$ | $P_{i1}$ | $P_{i2}$ |
|---|---|---|---|
| $D_1$ | 0.066 811 | −0.063 412 | 0.0 |
| $D_3$ | 4.528 30 | 0.956 790 | −1.214 491 |
| $D_4$ | 0.855 832 | −0.302 916 | 0.0 |
| $D_5$ | −0.002 459 | 0.002 260 | 0.0 |
| $D_7$ | 0.005 283 | −0.004 731 | 0.0 |
| | $Q_{i0}$ | $Q_{i1}$ | $Q_{i2}$ |
| $D_2^*$ | 0.0 | −0.041 271 | 0.017 332 |
| $D_6^*$ | 0.0 | −0.001 604 | 0.001 165 |
| $D_8^*$ | 0.0 | −0.003 834 | 0.001 210 |

### D. Transition dipole

The transition dipole moments and oscillator strengths from the ground to the first excited manifold ($n \rightarrow \sigma^*$) at the Franck–Condon (FC) region have been calculated. First, permanent dipole moments and transition dipole moments among spin-free states have been calculated with the spin-free CI, and then the transition dipoles including spin–orbit interaction have been calculated by multiplying spin-free dipoles by the contracted SOCI coefficients. The actual expression of the transition dipole between the ground state and excited state after contracted SOCI is given by

$$\mu_{IJ}=\sum\sum\ c_{Ii}c_{Jj}\langle {}^1i|\mu|{}^1j\rangle+\sum\sum\ c_{Ii}c_{Jj}\langle {}^3i|\mu|{}^3j\rangle, \tag{10}$$

where the summation covers three singlet [$^1i(A')$, $i=1$ to 3] and nine triplet [$^3i(A')$, $i=4$ to 12] states, and $c_{Jj}$, for instance, represents the contracted SOCI coefficient for spin–orbit free state $j$ in the SOCI state $J$.

### E. Classical trajectory calculation

The initial condition of 500 trajectories starting on the excited state was determined using the normal coordinates of the ground state, in the same way as was done in our previous paper.[48] The parent molecule $CH_3I$ (or $CD_3I$) is assumed to be in the ground rotational and vibrational state. The calculated normal frequencies, shown in Table III, are, as expected, on the average about 8.2% larger than the observed fundamental frequencies for both species.[54] Propagation of trajectories on the excited states and termination and analysis of trajectories were performed in the same way described in the previous paper.[48] We have also briefly examined the effect of using the more correct Wigner distribution for selection of initial conditions on the I*/(I*+I) branching ratio.

## III. RESULTS

### A. Transition moment at the Franck–Condon region

Table IV lists excitation energies, transition moments, and oscillator strengths from the ground to the first excited ($n \rightarrow \sigma^*$) manifolds at the ground state equilibrium geometry. The ratio of oscillator strengths for three allowed transitions, $^3Q_0$ (parallel), $^3Q_1$ (perpendicular), and $^1Q_1$ (perpendicular), is 0.81:0.17:0.02 and the parallel transition to $^3Q_0$ is the strongest, in qualitative agreement with experimental findings.[7,12,13] In the low energy region of $A$-band the character of the perpendicular transition to $^3Q_1$ should increase, in accord with the recent experimental report.[31,32] In the high energy region of $A$-band, the perpendicular transition to $^1Q_1$ becomes important. The situation is similar to that of ICN,[49] though the dependency of $CH_3I$ photodissociation dynamics on the excitation energy is not as clear as that of ICN.

### B. Features of the potential energy surfaces

In the previous paper, we discussed the PESs in detail with respect to both the umbrella angle and the bending

TABLE III. Calculated vibrational frequencies (in $cm^{-1}$) and their $L$ matrix.

| | | | |
|---|---|---|---|
| $CH_3I$ | | | |
| $a_1$ symmetry | 3 209.0 (2 933)[a] | 1 382.4 (1 252) | 566.8 (533) |
| $S_1$ | 0.998 150 | 0.007 634 | 0.011 275 |
| $S_2$ | 0.044 578 | 0.985 072 | 0.120 007 |
| $S_3$ | −0.041 344 | −0.171 973 | 0.992 709 |
| $e$ symmetry | 3 352.4 (3 060) | 1 591.7 (1 436) | 918.4 (882) |
| $S_4$ | 0.991 766 | −0.091 118 | 0.026 877 |
| $S_5$ | 0.123 139 | 0.975 789 | −0.190 501 |
| $S_6$ | −0.035 167 | 0.198 830 | 0.981 319 |
| $CD_3I$ | | | |
| $a_1$ symmetry | 2 300.6 (2 130)[a] | 1 083.5 (951) | 510.0 (501) |
| $S_1$ | 0.990 150 | −0.018 762 | 0.023 805 |
| $S_2$ | 0.107 727 | 0.951 801 | 0.303 692 |
| $S_3$ | −0.089 428 | −0.306 141 | 0.952 473 |
| $e$ symmetry | 2 506.5 (2 298) | 1 146.1 (1 049) | 681.1 (656) |
| $S_4$ | 0.979 163 | −0.115 842 | 0.038 676 |
| $S_5$ | 0.189 620 | 0.982 121 | −0.140 403 |
| $S_6$ | −0.072 697 | 0.148 388 | 0.989 339 |

Definition of symmetry coordinates[b]

| | | |
|---|---|---|
| $a_1$ | $CH_3$ $s$-str. | $S_1=1/\sqrt{3}(\Delta r_1+\Delta r_2+\Delta r_3)$, |
| | $CH_3$ $s$-def. | $S_2=1/\sqrt{6}(\Delta\alpha_1+\Delta\alpha_2+\Delta\alpha_3-\Delta\gamma_1-\Delta\gamma_2-\Delta\gamma_3)$, |
| | CI str. | $S_3=\Delta R$ |
| $e$ | $CH_3$ $d$-str. | $S_{4a}=1/\sqrt{6}(2\Delta r_1-\Delta r_2-\Delta r_3)$, |
| | | $S_{4b}=1/\sqrt{2}(\Delta r_2-\Delta r_3)$, |
| | $CH_3$ $d$-def. | $S_{5a}=1/\sqrt{6}(2\Delta\beta_1-\Delta\beta_2-\Delta\beta_3)$, |
| | | $S_{5b}=1/\sqrt{2}(\Delta\beta_2-\Delta\beta_3)$ |
| | $CH_3$ $d$-rock. | $S_{6a}=1/\sqrt{6}(2\Delta\alpha_1-\Delta\alpha_2-\Delta\alpha_3)$, |
| | | $S_{5b}=1/\sqrt{2}(\Delta\alpha_2-\Delta\alpha_3)$ |

[a]The numbers in the parentheses are observed fundamental frequencies from Ref. 54.

[b]$R$ is the distance between C and I atoms, $r_i$ is the distance between C and $H^i$ atoms, $\alpha_i$ is the angle of $H^iCI$ and $\gamma_i$ is the angle of $H^jCH^k$: $(i,j,k)=(1,2,3),(2,3,1),(3,1,2)$.

angle, important coordinates for the dynamics. In the present paper, we have used more flexible functional forms to cover very distorted geometries as well as the classically probed region. Thus the quantitative feature of the PESs changed somewhat, though the qualitative character remained unchanged. Therefore, we will briefly discuss again the PESs for umbrella and bending as well as for the newly added $CH_3$ stretchings.

Figure 2 shows the present $^3Q_0$ and $^1Q_1$ potential energy curves for the $C_{3v}$ symmetry. The $^1Q_1$ potential energy monotonically decreases in energy as $R$ increases. $^3Q_0$ has a shallow well of 0.212 eV at $R=6.233$ a.u. and $\alpha=93.9$ outside the conical intersection, in agreement with an estimation based on the $CH_3I$ (or $CD_3I$) photolysis experiment in rare gas matrix.[6]

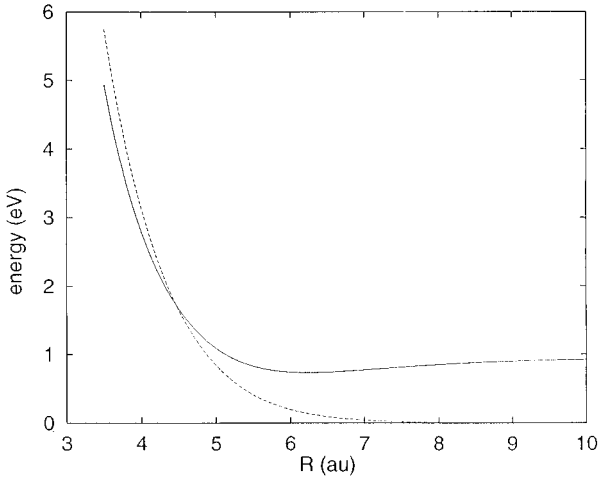


FIG. 2. Potential energy curves in the $C_{3v}$ symmetry with $\alpha$ optimized for each $R$ and $r_i$'s fixed to $r_e^\infty$. The solid curve is $^3Q_0$ and the dotted curve is $^1Q_1$.

The PES contour maps in the $C_{3v}$ symmetry are shown in Fig. 3, where the three CH distances are fixed to $r_e^\infty$. The coordinates used are

$$R_{\mathrm{tr}}=R-(m_x/m_{\mathrm{CX}})r_e^\infty\cos\alpha,$$
$$r_{\mathrm{int}}=-r_e^\infty\cos\alpha, \tag{11}$$

which diagonalize the kinetic energy operator.[48]

Figure 3 shows the PES contour maps in the new coordinate system, scaled with the proper mass so that the dynamics on these surfaces can be treated as that of a rolling ball. For $CH_3I$ in Figs. 3(a) and 3(b), the reaction coordinate (RC), the minima with respect to $r_{\mathrm{int}}$ for each $R_{\mathrm{tr}}$, on $^3Q_0$, passes the vicinity of the Franck–Condon geometry and intersects with $^1Q_1$ at $R_{\mathrm{tr}}=4.517$ and $r_{\mathrm{int}}=0.497$, i.e., $R=4.417$ and $\alpha=104.0$ deg. For $CD_3I$ in Figs. 3(c) and 3(d), the RC passes the region away from the Franck–Condon geometry, and the degrees of sudden switch of RC from $^3Q_0$ to $^1Q_1$ at the crossing substantially is larger than for $CH_3I$. In Fig. 3(d), RC of $^1Q_1$ passes through the region of $-0.17<r_{\mathrm{int}}<0$, i.e., $85<\alpha<90$ deg.

Figure 4 shows the potential energy curves with respect to the bending angle $\theta$ at various stages of dissociation. At the FC region, $^3Q_0$ surface has a minimum at $\theta=0$, whereas $^1Q_1$ surfaces have minima at $\theta=\pm3.6$ due to the Jahn–Teller distortion. At the conical intersection region, all three adiabatic surfaces have minima at a bent structure, with the largest bending stabilization of $\Delta E(\theta_{\min})=E(\theta_{\min})-E(0)=-7.87\times10^{-3}$ eV at $\theta_{\min}=5.6$. Outside the crossing region, $^3Q_0$ still has a positive bending force constant at $\theta=0$, while $^1Q_1$ surfaces become very flat with respect to $\theta$. As in the previous PESs,[48] this difference in the $\theta$ depen-

TABLE IV. Excitation energies, transition dipole moment, and oscillator strength at the equilibrium geometry.

| | Excitation energy (eV) | $\mu_x^a$ | $\mu_y^a$ | $\mu_z$ | Oscillator strength ($\times10^{-3}$) |
|---|---|---|---|---|---|
| $X\ ^1A_1(1A_1)\rightarrow{}^3Q_1(2E)$ | 4.657 | 0.0159 | 0.0159 | 0.0 | 0.06 |
| $X\ ^1A_1(1A_1)\rightarrow{}^3Q_{0-}(1A_2)$ | 5.008 | 0.0 | 0.0 | 0.0 | 0.0 |
| $X\ ^1A_1(1A_1)\rightarrow{}^3Q_{0+}(2A_1)$ | 5.120 | 0.0 | 0.0 | 0.1531 | 2.93 |
| $X\ ^1A_1(1A_1)\rightarrow{}^1Q_1(3E)$ | 5.457 | 0.0481 | 0.0481 | 0.0 | 0.61 |

[a]For degenerate transition, both $A'(x)$ and $A''(y)$ components are given.

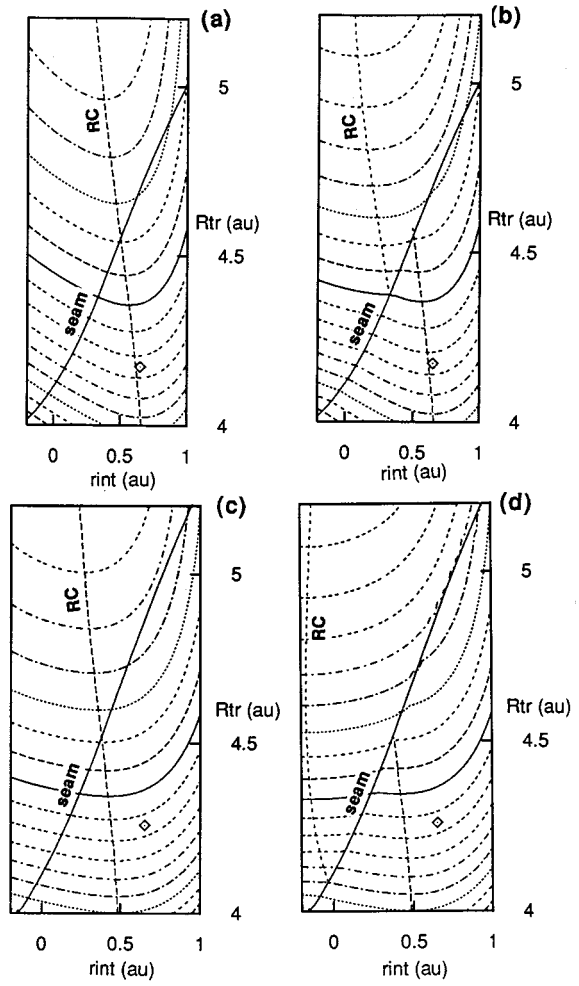


FIG. 3. Contour maps of potential energy surfaces with respect to $R_{tr}$ and $r_{int}$. (a) $^3Q_0$ of $CH_3I$, (b) $^3Q_0 \rightarrow {}^1Q_1$ of $CH_3I$, (c) $^3Q_0$ of $CD_3I$, (d) $^3Q_0 \rightarrow {}^1Q_1$ of $CD_3I$. Label seam represents the conical intersection between $^3Q_0$ and $^1Q_1$. Labels RC and $\diamond$ represent the reaction coordinate and the ground state equilibrium (Franck–Condon) geometry, respectively. The contour spacing is 0.2 eV.

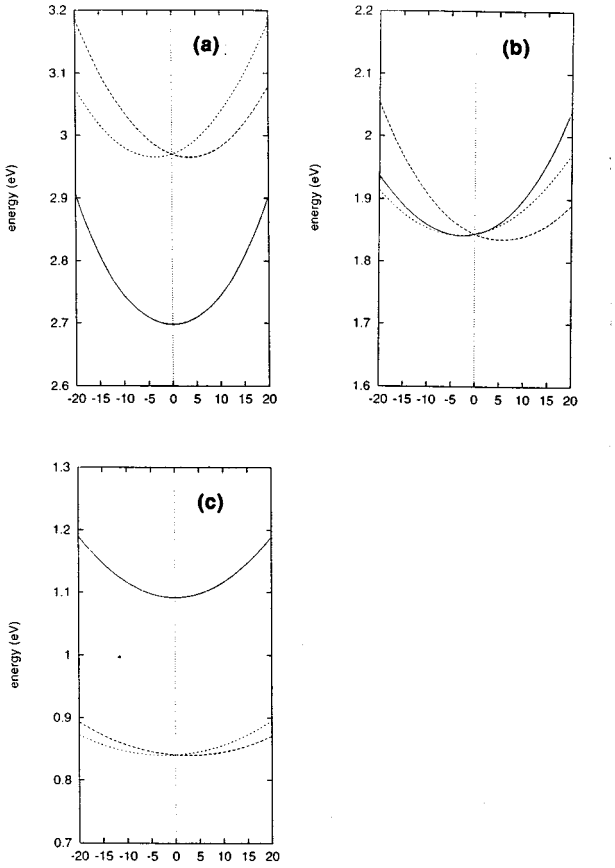


FIG. 4. Adiabatic potential energy curves with respect to $\theta$ at (a) the FC region, $R=4.040\,95$ a.u., $\theta=108.5°$; (b) the conical intersection, where the $^3Q_0$ reaction coordinate crosses $^1Q_1$, $R=4.417$, $\theta=104.0°$; and (c) outside the conical intersection, $R=5.0$, $\theta=102.0°$ for $^3Q_0$, $\theta=99.0°$ for $^1Q_1$. The local symmetry of $CH_3$ ($r_i=r_e^{\infty}$) is assumed to be $C_{3v}$. $\alpha$ is optimized at each $R$ for each state for (c). The positive and negative values of $\theta$ in these figures represent $\phi=0$ and $\pi$, respectively. The solid line is the curve of which main component is $^3Q_0(A')$, the dashed line is that for $^1Q_1(A')$, and the dotted line is that for $^1Q_1(A'')$.

dence between the $^1Q_1$ and $^3Q_0$ surfaces is the most important factor determining the energy partitioning into the $CH_3$ ($CD_3$) rotation.

Next we describe the PESs with respect to three CH stretching coordinates. Both $^3Q_0$ and $^1Q_1$ adiabatic PESs with respect to the degenerate $CH_3$ stretching coordinates, $S_{4a}$ and $S_{4b}$ are almost the same as the corresponding part of $V_{CH_3}$ at the dissociation limit. As discussed in Sec. II C, there is no numerical dependency on either coordinate in the diabatic diagonal terms and the small dependency of the off-diagonal terms, $V_{13}$ and $V_{23}$ has little effect. On the other hand, the adiabatic PESs with respect to the symmetric $CH_3$ stretching coordinate $S_1$ are different from that of $V_{CH_3}$, because the diabatic diagonal terms have first order terms in $S_1$, as shown in Eqs. (2)–(4) in Sec. II C. Figure 5 show the PESs with respect to $S_1$. At the FC region, the CH distance is longer ($S_{1min}=0.0498$ or $r_{CH}=2.0814$) than in the ground state ($S_1=0.0226$ or $r_{CH}=2.0657$), which in turn is longer than in the $CH_3$ fragment ($S_1=0$ or $r_{CH}=2.0527$). There is an energy difference $\Delta E(S_{1min})=E(S_{1min})-E(S_1=0)$ of about 0.01 a.u. between $S_{1min}$ and $S_1=0$. As the dissociation proceeds, the CH distance smoothly approaches the $CH_3$ value. The calculated values of $S_{1min}$ and $\Delta E(S_{1min})$ are shown in Table V. This behavior of PESs with respect to $S_1$ is related to the mechanism of symmetric stretching excitation of the $CH_3$ product, as will be discussed later in detail.

Finally, we briefly describe the PESs with respect to the $CH_3$ deformation coordinates, $S_5$'s. The $^3Q_0$ surface with respect to these coordinates is almost the same as that of $V_{CH_3}$, as the diabatic $V_3$ term has no dependency and the off-diagonal contributions from $V_{12}$, $V_{13}$, and $V_{23}$ are small. On the other hand, the diabatic $V_1$ and $V_2$ have $S_{5a}$-dependency, which increases $V_1$ and decreases $V_2$ as $S_{5a}$ increases. This dependency, however, does not play an important role in the dynamics.

### C. I*/(I*+I) branching ratio

In our previous classical trajectory results on six-dimensional PESs, when the trajectories are started on the

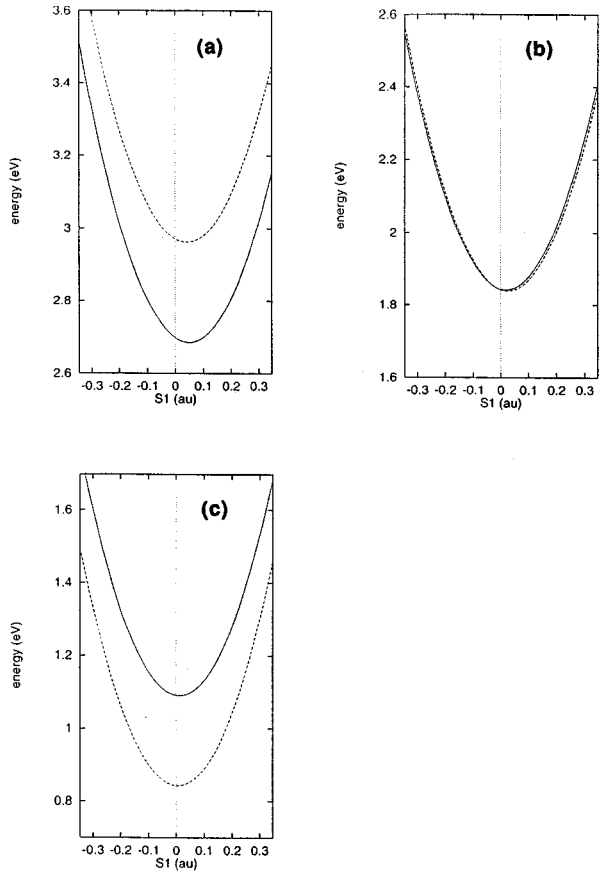


FIG. 5. Adiabatic potential energy curves with respect to symmetric stretch coordinate $S_1$ at (a) the FC region, (b) the conical intersection, (c) outside the conical intersection. $R$ and $\alpha$ for each figure are same as those in Fig. 4. The symmetry of $CH_3I$ ($r_i=r_e^{\infty}$) is assumed to be $C_{3v}$. The solid line is the curve of $^3Q_0$ and the dotted line is that of $^1Q_1$.

$^3Q_0$ PES, we have obtained the I*/(I*+I) branching ratio of 0.91 vs experimental ~0.7.[48] This was the most notable disagreement of the calculated results in comparison with a variety of experimental findings. We have suggested that this discrepancy is possibly caused by the fact that three CH stretching coordinates were frozen in our study. In the present trajectory study, where all the internal degrees of freedom of $CH_3I$ are included, we have obtained an I*/(I*+I) ratio of 0.83. This changes to 0.87 when the Wigner initial conditions are used. As mentioned in Sec. III A, the direct transition to $^1Q_1$ is not negligible and we have averaged the branching ratios calculated by starting trajectories on $^3Q_0$ and $^1Q_1$ with the ratio of 0.81:0.17 (cf. Sec. III A) and obtained 0.72. One should note that the vibrational frequencies of $CH_3I$ are so high that the population of vibrationally excited states is never important in most photodissociation experiments. This is in contrast to the situation for ICN photodissociation, where initial vibrational excitation of ICN is important for discussion of the dynamics.[49]

TABLE V. Stabilization energy $\Delta E^a$ (in eV) with respect to $S_1$.

| | | $\Delta E(S_{1\min})\times 10^{-3}$ | |
|---|---|---|---|
| $R$ | $\alpha$ | $^3Q_0$ | $^1Q$ |
| 4.040 95 | 108.5 | 12.899(0.050) | 9.303(0.042) |
| 4.417 | 104.0 | 3.425(0.026) | 1.891(0.019) |
| 5.0 | 102.0[b] | 0.627(0.010) | ⋯ |
| | 99.7[b] | ⋯ | 0.131(0.005) |

[a]$\Delta E$ is defined by $\Delta E(S_{1\min})-\Delta E(S_1=0)$.
[b]Optimized $\alpha$ for each state.

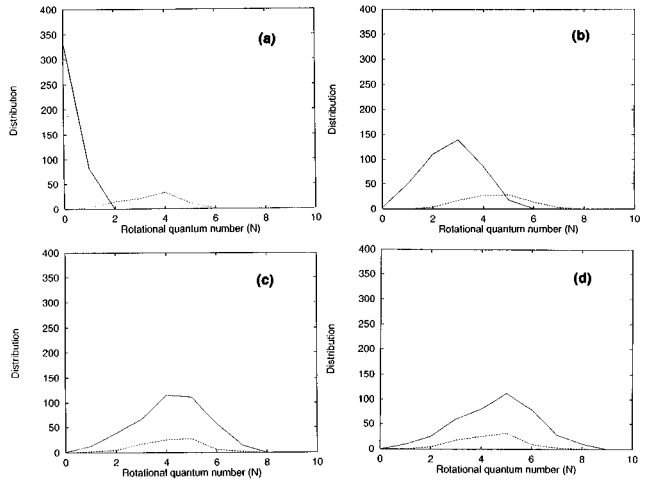


FIG. 6. The rotational distribution of (a) $CH_3$ and (b) $CD_3$ for the final state, (c) $CH_3$, and (d) $CD_3$ at the transition state. The solid line is the distribution of the I*-channel products and the dotted line is that of the I-channel products.

We have calculated the I*/(I*+I) branching ratio for $CD_3I$ photodissociation to be 0.82 (0.80 with Wigner initial conditions) when trajectories are started on $^3Q_0$, and 0.73 when the contribution of direct excitation to $^1Q_1$ is considered. The calculated branching ratio is not sensitive to the mass, whereas experiments indicate a significant mass effect, ~0.7 for $CH_3I$, ~0.8 for $CD_3I$. Since surface hopping trajectories may not be the most reliable ways of obtaining the branching ratio, we are planning to perform quantum dynamic calculations for more rigorous comparison.[55]

Since the contribution of the direct excitation to the $^1Q_1$ state is relatively small, in the following subsections, all the discussions on the dynamics will be made solely based on trajectories starting on $^3Q_0$.

### D. Rotational excitation

In our previous 6D trajectory study, we have obtained a reasonable agreement with experiments concerning the rotational distribution of the $CH_3$ product; in the I-channel $CH_3$ is rotationally excited around the axis perpendicular to its top axis, while in I*-channel it is rotationally cold.[48] The results with the new 9D trajectories are shown in Fig. 6. Figure 6(a) gives the rotational distribution of the $CH_3$ fragment. The distribution of the I-channel product has a peak at $N=4$ and that of the I*-channel is colder with a maximum at $N=0$. This can be compared with our 6D results, the I-channel peak at $N=5$ and the I*-channel at $N=1$; the latter peak is considered to be spurious due to the three frozen CH degrees of freedom. The mechanism of rotational excitation is quali-

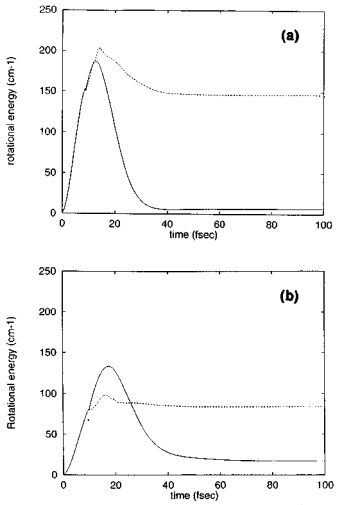


FIG. 7. Plots of time vs the rotational energy of (a) $CH_3$ and (b) $CD_3$ for a randomly selected trajectory. The solid line represents a trajectory which stayed on $^3Q_0$ to give the I* channel product. The dotted line is the same trajectory but was forced to switch to $^1Q_1$ to give the I channel product.

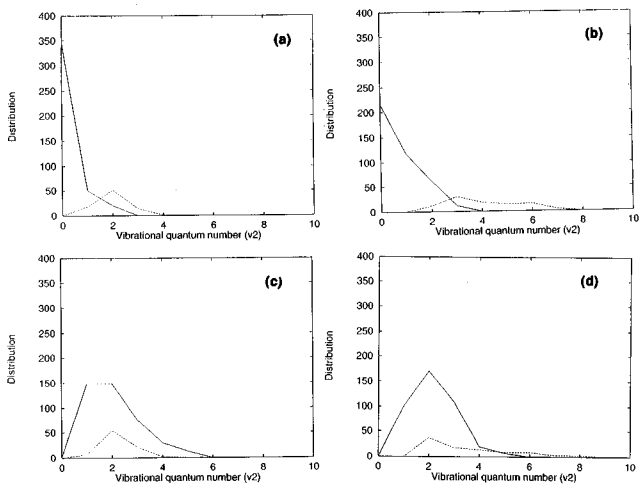


FIG. 8. The vibrational distribution of the umbrella mode of (a) $CH_3$ and (b) $CD_3$ for the final state, (c) $CH_3$ and (d) $CD_3$ at the transition state. Glossaries are the same as in Fig. 6.

tatively the same as before. Figure 7 shows the plots of rotational energy as functions of time. Before a trajectory reaches the conical intersection region, the rotation is quickly excited because of zero-point $CH_3$ degenerate rocking vibration on the steep $^3Q_0$ surface. After the conical intersection, the trajectory that made a transition to $^1Q_1$ maintains the rotational energy up to the I-channel dissociation limit, while the one that stayed on $^3Q_0$ loses rotation quickly. This difference behaviors are dictated by different shapes of PESs, as discussed in Sec. III B.

Figure 6(b) shows the rotational distribution of the $CD_3$ fragment. The distributions have peaks at $N=5$ for the I-channel and $N=3$ for the I*-channel, respectively. Both of distributions peaks are shifted up by one and three angular momentum units, respectively, compared with those of the $CH_3$ fragment. This is in qualitative agreement with experimental findings.[21,22,24] For instance, Chandler *et al.* estimated the average of the rotational energy to be 104 $cm^{-1}$ for $CH_3$ and 94 $cm^{-1}$ for $CD_3$, in terms of angular momentum units, $N=3-4$, and $N=4-5$, respectively. The reason for the higher rotational angular momentum of $CD_3$ fragment may be justified as follows. $CD_3I$ is heavier than $CH_3I$ and takes longer to reach the crossing region, accumulating more angular momentum. After the crossing region, the rotation is suppressed either on $^1Q_1$ or on $^3Q_0$, though by different degrees. Since the moment of inertia around the perpendicular axis is larger for $CD_3$, on whichever PES, the degree of rotational dumping would be smaller, leaving a larger angular momentum in the product than for $CH_3$.

### E. Vibrational excitation of umbrella mode

As shown in Fig. 8(a), the vibrational distributions of the $CH_3$ umbrella mode reproduce the experimental $I^*/(I^*+I)$ channel selectivity very well. The origin of the selectivity is exactly the same as before.[48] As shown in Fig. 3(a) a trajectory in the I*-channel starting from the Franck–Condon excitation travels around the RC up to the dissociation limit and therefore the geometrical relaxation from the $C_{3v}$ to $D_{3h}$ structure takes place gradually and no vibrational excitation is expected. However, a trajectory to dissociate in the I-channel experiences a sudden change in PES at the conical intersection region, i.e., the RC at $r_{\mathrm{int}}\sim 0.1$ on $^3Q_0$ switches to the RC at $r_{\mathrm{int}}\sim 0.0$ on $^1Q_1$, and a large vibrational excitation takes place instantaneously.

Figure 8(b) shows the distribution of the $CD_3$ umbrella mode. The populations of the vibrationally excited products for both I and I* channels are larger than those of the $CH_3$ fragment. As seen in Figs. 3(a) and 3(c) the RC on $^3Q_0$ is farther away from the Franck–Condon geometry for $CD_3I$ than for $CH_3I$. Thus the umbrella vibration quantum number is expected to be larger for $CD_3I$ than for $CH_3I$ by the time trajectories on $^3Q_0$ reach the crossing region, which is actually seen in comparison of Figs. 8(c) and 8(d). Another factor why the umbrella mode of the $CD_3$ fragments for both I* and I channels are more vibrationally excited than those of the $CH_3$ is a heavier mass of $CD_3$. That is, the heavier fragments of $CD_3$ is harder to be relaxed.

### F. Vibrational excitation of symmetric stretching mode

In the present calculation, all of trajectories give the $CH_3$ (and $CD_3$) products in $v_1=0$ of the symmetric stretching mode. However, our present classical treatment of the vibrational quantum number of assigning the quantum number zero for vibrational energies of up to $1.0h\nu_1$ may not be appropriate, and at least the distribution of high frequency modes should be treated quantum mechanically. Such a quantum mechanical study is progress in collaboration with Hammerich and Kosloff.[55] Here we will give a classical evidence that the average energy is more than $0.5h\nu_1$ in the product. In Table VI, we show the average of the vibrational energy in the symmetric stretch mode at the conical interac-

TABLE VI. The average vibrational energy of the symmetric stretching mode (in $cm^{-1}$).

| | $CH_3I$ (reactant) | $CH_3I$ (TS)[a] | $CH_3$ (product) |
|---|---|---|---|
| I* | 1605 | 2444 | 2049 |
| I | 1605 | 2424 | 2093 |
| | $CD_3I$ (reactant) | $CD_3I$ (TS) | $CD_3$ (product) |
| I* | 1150 | 1824 | 1520 |
| I | 1150 | 1965 | 1603 |

[a]At the conical intersection.

tion region and in the product $CH_3$ ($CD_3$) in both I and I* channel. We have assumed that the parent molecules are all in the ground vibrational state, with the symmetric stretch vibrational energy of $0.5h\nu_1=1605$ (1150) $cm^{-1}$. It can be seen that $CH_3$ (and $CD_3$) gains the symmetric stretching energy during the photodissociation with little channel selectivity. Actually 2049 (1520) and 2093 (1603) $cm^{-1}$ energy of the product $CH_3$ ($CD_3$) correspond to the vibrational quantum number $v_1=0.65$ [0.68 and 0.66 (0.71), respectively]. As is seen in Table VI, the symmetric stretch energy at the conical intersection region is substantially larger than in the ground state reactant. At the Franck–Condon region, the optimal $S_1$ value in the excited state is different from in the ground state, as discussed in Sec. III B, and this gives some $S_1$ vibrational excitation. As the molecules travel down the steep dissociation pathway to the conical intersection region, the released potential energy is transferred in part to this mode, as well as to some other modes. After the conical intersection region, the potential energy release is small and the vibrational energy in the $S_1$ mode is dissipated into translation and other modes. The shapes of $^3Q_0$ and $^1Q_1$ PESs with respect to $S_1$ are similar and trajectories on both PESs behave similarly as to the $S_1$ vibration, resulting in virtually no channel specificity on the symmetric stretch energy in the product.

## IV. CONCLUDING REMARKS

In the present study, we calculated the potential energy surfaces and transition dipole by means of the *ab initio* contracted SOCI calculations. The full nine-dimensional potential energy functions, including the previously missing three CH stretching degrees of freedom, are derived. Surface hopping quasiclassical trajectory calculation on them reproduces important recent experimental findings of $CD_3I$ as well as $CH_3I$ photodissociation.

The transition intensity is a mixture of parallel and perpendicular components with a ratio of oscillator strength of 81:19. Although the parallel transition to the $^3Q_0$ state is dominant, the perpendicular transition intensity to $^1Q_1$ (and $^3Q_1$) is not negligibly small, in agreement with the recent experimental findings. The perpendicular transition to $^1Q_1$ has to be taken into account to obtain a reasonable I*/(I*+I) branching ratio.

The rotational distribution of the $CH_3$ fragments reproduces the experimental findings; the I-channel product is hot with a peak at $N=4$, on the other hand, the I*-channel product is much colder with a maximum at $N=0$. The mechanism of the rotational excitation and its channel selectivity closely relates to the shape of the PESs with respect to the bending angle outside the conical intersection. The $CD_3$ product has a higher rotational excitation than the $CH_3$ product, in agreement with experiments, which can be explained by considering two factors, (i) the shape of the bending PESs outside the conical intersection region, and (ii) the difference in the moment of inertia between $CH_3$ and $CD_3$.

The vibrational distribution of the umbrella mode of $CH_3$ ($CD_3$) is determined by the shape of the PESs with respect to the umbrella angle and its coupling with the CI distance $R$. In the I-channel product the product is vibrationally hot due to the sudden change of the RC from $^3Q_0$ to $^1Q_1$ at the conical intersection. The experimental results that both I* and I channel products of $CD_3$ have hotter distributions than those of $CH_3$ is mainly due to the fact that the RC on the $^3Q_0$ of $CD_3I$ is farther away from the Franck–Condon geometry than that of $CH_3I$.

Trajectory calculation gives the $CH_3$ and $CD_3$ product all in the ground symmetric stretching state, if classical vibrational numbers are truncated. However, the average symmetric stretching energy is substantially increased from $0.5h\nu_1$ to $0.65-0.7h\nu_1$. A more reliable quantum mechanical calculation will be needed to examine the possibility of the $\nu_1=1$ excited state in the product.

Thus with the new nine-dimensional PESs and surface-hopping trajectories, we were able to explain experimental results better than the previous six-dimensional PESs. We could also explain most of the experiments for $CD_3I$ photodissociation as well. However, in order to discuss the dynamics in detail, we have to treat the motion of the nuclei on the nine-dimensional PESs quantum mechanically. Such a work is now in progress with Kosloff and Hammerich and will be published elsewhere.[55]

The largest deficiency of our previous 6D PESs as well as the new 9D PESs is in the Franck–Condon region, where the calculated $X \rightarrow {}^3Q_0$ vertical excitation energy of 5.12 eV is too large compared with the experiment of 4.7 eV and the PES is too steep to reproduce the width of the absorption spectrum.[42,55] Various modifications of PESs to improve agreement with experiments have been examined extensively and will be published elsewhere.

## ACKNOWLEDGMENTS

We would like to acknowledge Dr. Kosloff and Dr. Hammerich for valuable comments and discussions. All the *ab initio* calculations were carried out at the IMS computer center. Y.A. and S.Y. thank Grants-in-Aid for Scientific Research in the Priority Area of ''Theory of Chemical Reactions'' from the Ministry of Education, Culture, and Science of Japan. K.M. is grateful to a grant from the Air Force Office of Scientific Research, F49620-95-1-0182.

## APPENDIX

Considering the three factors, (i) the numerical behavior of the diabatic terms, (ii) the requirement that the adiabatic $^3Q_0$ and $^1Q_1$ energies are invariant under permutation among three hydrogen atoms, and (iii) the fact that the force field of $CH_3$ in the dissociation limit, $V_{CH_3}$, in each diagonal term satisfies the requirement (ii), the fitting functions except for $V_{CH_3}$ and the constant $\Delta E_I$ are assumed to have the forms shown in Eqs. (A1)–(A6),

$$V_1 = V_{10} + P_1 X + P_2 S_{5a}, \tag{A1}$$

$$V_2 = V_{10} - (P_1 X + P_2 S_{5a}), \tag{A2}$$

$$V_3 = V_{30}, \tag{A3}$$

$$V_{12} = P_1 Y + P_2 S_{5b}, \tag{A4}$$

$$V_{13} = Q_1 X + Q_2 S_{5a} + Q_3 S_{4a}, \tag{A5}$$

$$V_{23} = -(Q_1 Y + Q_2 S_{5b} + Q_3 S_{4b}), \tag{A6}$$

where $V_{10}$, $V_{30}$, $P_1$, $P_2$, $Q_1$, $Q_2$, and $Q_3$ are functions with respect to $R$, $\alpha$, $\theta$, and $S_1$, which are invariant under permutation, and $S_1$, $S_{4a}$, $S_{4b}$, $S_{5a}$, $S_{5b}$, $X$, and $Y$ are defined by Eqs. (A7)–(A9), where

$$\begin{aligned}
&S_1 = (1/\sqrt{3})(\Delta r_1 + \Delta r_2 + \Delta r_3),\\
&S_{4a} = (1/\sqrt{6})(2\Delta r_1 - \Delta r_2 - \Delta r_3),\\
&S_{4b} = (1/\sqrt{2})(\Delta r_2 - \Delta r_3),\\
&\Delta r_i = r_i - r_e^{\infty} \quad (i = 1,2,3),\\
&S_{5a} = (1/\sqrt{6})(2\Delta\beta_1 - \Delta\beta_2 - \Delta\beta_3),\\
&S_{5b} = (1/\sqrt{2})(\Delta\beta_2 - \Delta\beta_3),\\
&\Delta\beta_i = \beta_i - 2\pi/3 \quad (i = 1,2,3),
\end{aligned} \tag{A7}$$

$$X(\phi,\beta_2,\beta_3,\zeta) = \{\cos(3\phi+\zeta) + \cos[3(\phi+\beta_3)+\zeta] + \cos[3(\phi-\beta_2)+\zeta]\}/3, \tag{A8}$$

$$Y(\phi,\beta_2,\beta_3,\zeta) = \{\sin(3\phi+\zeta) + \sin[3(\phi+\beta_3)+\zeta] + \sin[3(\phi-\beta_2)+\zeta]\}/3, \tag{A9}$$

$$\begin{aligned}
&\tan\zeta = \tan(\zeta_1 + \zeta_2),\\
&\tan\zeta_1 = S_{5b}/S_{5a},\\
&\tan\zeta_2 = S_{4b}/S_{4a}.
\end{aligned} \tag{A10}$$

The reason why $V_3$ has a simple form $V_{30}$ in Eq. (A3) is that $B_9$, $B_{10}$, and $B_{11}$ in Eq. (4) are zero.

A set of dihedral angels $A = \{\phi, \phi+\beta_3, \phi-\beta_2\}$ are defined by those of the I atom against the three hydrogen atoms $H^1$, $H^2$, and $H^3$, respectively (cf. Fig. 1). If one permutes two hydrogens, one would obtain another set of angles $A' = \{\phi', \phi' + \beta_3', \phi - \beta_2'\}$. However, two sets $A$ and $A'$ are identical.

Next we comment on the phase factor $\zeta$ in $X$ (and $Y$). The secular equation composed of Eqs. (A1)–(A6) gives a cubic equation in (A11),

$$\begin{aligned}
&x^3 - (2V_{10}+V_{30})x^2 + [-(V_{10}^2 + 2V_{30}V_{10}) + (P_1^2+Q_1^2)(X^2+Y^2) + Q_3^2(S_{4a}^2+S_{4b}^2) + (P_2^2+Q_2^2)(S_{5a}^2+S_{5b}^2)\\
&\quad + 2Q_2Q_3(S_{4a}S_{5a}+S_{4b}S_{5b}) + 2(P_1P_2+Q_1Q_2)(XS_{5a}+YS_{5b}) + 2Q_1Q_3(XS_{4a}+YS_{4b})]x\\
&\quad - [V_1V_2V_3 - (V_1V_{23}^2 + V_2V_{13}^2 + V_3V_{12}^2) + 2V_{12}V_{23}V_{13}] = 0.
\end{aligned} \tag{A11}$$

In order to satisfy the energy invariance under permutation, the coefficients of the cubic equation have to satisfy the invariance under permutation. The coefficients of the second order and the first to fifth coefficients of the first order are invariant. If one chooses the phase factor $\zeta$ determined by Eq. (A10), the sixth and seventh coefficient of the first order in Eq. (A11), $2(P_1P_2+Q_1Q_2)(XS_{5a}+YS_{5b})$ and $2Q_1Q_3(XS_{4a}+YS_{4b})$, respectively, are possible to be simultaneously invariant due to the fact that the dihedral angle set $A$ is invariant. It can be also proved that the constant term is invariant under permutation.


[1] J. V. V. Kasper and G. C. Pimentel, Appl. Phys. Lett. **5**, 231 (1964).
[2] S. J. Riley and K. R. Wilson, Faraday Discuss. Chem. Soc. **53**, 132 (1972).
[3] M. J. Dzvonik and S. C. Yang, Rev. Sci. Instrum. **45**, 750 (1974).
[4] M. J. Dzvonik, S. C. Yang, and R. Bersohn, J. Chem. Phys. **61**, 4408 (1974).
[5] A. Gedanken and M. D. Rowe, Chem. Phys. Lett. **34**, 39 (1975).
[6] L. E. Brus and V. E. Bondybey, J. Chem. Phys. **65**, 71 (1976).
[7] T. F. Hunter and K. S. Kristjansson, Chem. Phys. Lett. **58**, 291 (1978).
[8] R. K. Sparks, K. Shobatake, L. R. Carlson, and Y. T. Lee, J. Chem. Phys. **75**, 3838 (1981).
[9] S. L. Baughcum and S. R. Leone, J. Chem. Phys. **72**, 6531 (1980).
[10] H. W. Hermann and S. R. Leone, J. Chem. Phys. **76**, 4766 (1982).
[11] W. P. Hess, S. J. Kohler, H. K. Haugen, and S. R. Leone, J. Chem. Phys. **84**, 2143 (1986).
[12] M. D. Barry and P. A. Gorry, Mol. Phys. **52**, 461 (1984).
[13] G. N. A. van Veen, T. Baller, A. E. de Vries, and N. J. A. van Veen, Chem. Phys. **87**, 405 (1984).
[14] M. O. Hale, G. E. Galica, S. G. Glogover, and J. L. Kinsey, J. Phys. Chem. **90**, 4997 (1986).
[15] J. F. Black and I. Powis, Chem. Phys. Lett. **148**, 479 (1988).
[16] J. F. Black and I. Powis, Laser Chem. **9**, 339 (1988).
[17] J. F. Black and I. Powis, Chem. Phys. **125**, 375 (1988).
[18] J. F. Black and I. Powis, Chem. Phys. **89**, 3986 (1988).
[19] I. Powis and J. F. Black, J. Phys. Chem. **93**, 2461 (1989).
[20] D. W. Chandler and P. L. Houston, J. Chem. Phys. **87**, 1445 (1987).
[21] D. W. Chandler, J. W. Thoman, Jr., M. H. M. Janssen, and D. H. Parker, Chem. Phys. Lett. **156**, 151 (1989).
[22] D. W. Chandler, M. H. M. Janssen, S. Stolte, R. N. Strickland, J. W. Thoman, Jr., and D. H. Parker, J. Phys. Chem. **94**, 4839 (1990).
[23] R. O. Loo, G. E. Hall, H. P. Haerri, and P. L. Houston, J. Phys. Chem. **92**, 5 (1988).

[24] R. O. Loo, H. P. Haerri, G. E. Hall, and P. L. Houston, J. Chem. Phys. **90**, 4222 (1989).
[25] K. Q. Lao, M. D. Person, P. Xayariboun, and L. J. Butler, J. Chem. Phys. **92**, 823 (1990).
[26] M. D. Person, P. W. Kash, and L. J. Butler, J. Chem. Phys. **94**, 2557 (1991).
[27] T. Suzuki, H. Kanamori, and E. Hirota, J. Chem. Phys. **94**, 6607 (1991).
[28] T. J. Sears, J. Frye, V. Spirko, and W. P. Kraemer, J. Chem. Phys. **90**, 2125 (1989).
[29] G. E. Hall, T. J. Sears, and J. M. Frey, J. Chem. Phys. **90**, 6234 (1989).
[30] M. Zahedi, J. A. Harrison, and J. W. Nibler, J. Chem. Phys. **100**, 4043 (1994).
[31] D. H. Fairbrother, K. A. Briggman, E. Weitz, and P. C. Stair, J. Chem. Phys. **101**, 3787 (1994).
[32] R. A. Hertz and J. A. Syage, J. Chem. Phys. **100**, 9625 (1994).
[33] (a) L. C. Pipes, D. Y. Kim, N. Brandstater, C. D. Fugelsnag, and D. Baugh, Chem. Phys. Lett. **219**, 207 (1994); (b) D. Y. Kim, N. Brandstater, L. C. Pipes, T. Garner, and D. Baugh, J. Phys. Chem. **99**, 4364 (1995).
[34] A. Strobel, I. Fischer, A. Lochschmidt, K. M. Dethlefs, and V. E. Bondybey, J. Phys. Chem. **98**, 2024 (1994).
[35] (a) M. Shapiro and R. Bersohn, J. Chem. Phys. **73**, 3810 (1980); (b) S. Kanfer and M. Shapiro, J. Phys. Chem. **88**, 3964 (1984).
[36] M. Shapiro, J. Phys. Chem. **90**, 3644 (1986).
[37] S. Lee and E. J. Heller, J. Chem. Phys. **76**, 3035 (1982).
[38] D. Imre, J. L. Kinsey, A. Sinha, and J. Krenos, J. Phys. Chem. **88**, 3956 (1984).
[39] R. L. Sundberg, D. Imre, M. O. Hale, J. L. Kinsey, and R. D. Coalson, J. Phys. Chem. **90**, 5001 (1986).
[40] (a) H. Guo and G. C. Schatz, J. Chem. Phys. **93**, 393 (1990); (b) J. Phys. Chem. **95**, 3091 (1991).
[41] H. Guo, K. Q. Lao, G. C. Schatz, and A. D. Hammerich, Journal **94**, 6562 (1991).
[42] (a) H. Guo, J. Chem. Phys. **96**, 2731 (1992); (b) **96**, 6629 (1992).
[43] M. R. Wedlock and K. F. Freed, J. Chem. Phys. **95**, 7275 (1991).
[44] (a) M. H. Alexander, C. Rist, and D. E. Manolopoulos, J. Chem. Phys. **97**, 4836 (1992); (b) C. Rist and M. H. Alexander, *ibid*. **98**, 6196 (1993).
[45] S. M. Miller and M. H. Alexander, J. Chem. Phys. **101**, 8663 (1994).
[46] M. Tadjeddine, J. P. Flament, and C. Teichteil, Chem. Phys. **118**, 45 (1987).
[47] S. Yabushita and K. Morokuma, Chem. Phys. Lett. **153**, 517 (1988).
[48] Y. Amatatsu, K. Morokuma, and S. Yabushita, J. Chem. Phys. **94**, 4858 (1991).
[49] Y. Amatatsu, S. Yabushita, and K. Morokuma, J. Chem. Phys. **100**, 4894 (1994).
[50] U. Manthe and A. D. Hammerich, Chem. Phys. Lett. **211**, 7 (1993).
[51] A. D. Hammerich, U. Manthe, R. Kosloff, H. D. Meyer, and L. S. Cederbaum, J. Chem. Phys. **101**, 5623 (1994).
[52] (a) R. Shepard, I. Shavitt, R. M. Pitzer, D. C. Comeau, M. Pepper, H. Lischka, P. G. Szalay, R. Ahlrichs, F. B. Brown, and J. G. Zhao, Int. J. Quantum. Chem. Symp. **22**, 149 (1988); (b) IMS Computor Center Library, implemented by S. Yabushita.
[53] Hammerich *et al.* made a comment on our transformation, which was that two diabatic states $^1\Phi_1$ and $^1\Phi_2$ can be further transformed into potential energy surfaces and elimination of any $\phi$ dependence, though we did not transform into them (see Ref. 51).
[54] *Tables of Molecular Vibrational Frequencies*, edited by T. Shimanouchi (U.S. GPO, Washington, D.C., 1972), Vol. 1.
[55] A. D. Hammerich, R. Kosloff, Y. Amatatsu, and K. Morokuma (unpublished).